Bottom-up construction of highly photoactive dye-sensitized titania using Ru(II) and Ir(III) complexes as building blocks

Marisa Rico-Santacruz[a], Ángel E. Sepúlveda[b], Cintia Ezquerro[b], Elena Serrano[a], Elena Lalinde[b], Jesús R. Berenguer[b,*], Javier García-Martínez[a,*]

[a] Departamento de Química Inorgánica-Laboratorio de Nanotecnología Molecular, Universidad de Alicante, Carretera San Vicente s/n, E-03690 Alicante, Spain[1]
[b] Departamento de Química-Centro de Investigación en Síntesis Química (CISQ), Universidad de La Rioja Madre de Dios, 54, E-26006, Logroño, La Rioja, Spain

ABSTRACT

The one-pot co-condensation of tetrabutyl orthotitanate (TBOT) and the neutral Ru(II) N3 dye or the new cationic Ir(III) complex [Ir(ppy)$_2$(3,3′-H$_2$dcbpy)]PF$_6$ have yielded novel hybrid *in-situ* titanias, which present an exceptional stability against leaching or photodegradation of the coordination dye. The main advantages of this strategy are: i) high dye incorporation level, ii) narrowing band gap and iii) high stability. These materials exhibit much higher photocatalytic activity, under both UV and visible light, not only than the dye-free titania but also than the related dye-sensitized titania prepared by post-synthetic grafting. This *in-situ* synthetic approach is a promising alternative route to prepare highly stable dye-sensitized materials with great applicability potential.

© 2016 Elsevier B.V. All rights reserved.

1. Introduction

The quest for materials able to efficiently harvest solar light has become one of the biggest challenges of our time. Among the most promising materials, TiO$_2$ has emerged as one of the most suitable candidates [1–4], despite presenting some drawbacks. Thus, it presents a high electron-hole recombination range and, because of its large band gap (3.2 eV for its anatase phase), is able to capture only 4–5% of the solar spectrum [5–7]. Therefore, reducing its band gap is an important goal towards unlocking the potential of TiO$_2$ in visible light utilization.

Among the different strategies developed for improving its efficiency, photosensitization via surface functionalization with organic or inorganic dyes [6,8–12] has received increasing attention in recent years. In most of the systems, the photosensitizer is able not only to inject electrons into the conduction band of TiO$_2$ upon absorption of visible light, but also to control the charge separation and recombination dynamics at the sensitizer/nanocrystals interfaces [13–15]. As a result, the anchorage through the interface becomes of critical importance.

Dye-sensitized titanias have proven to be very efficient in photovoltaic systems, such as dye-sensitized solar cells (DSSCs) [8–10,12,16], and have shown enhanced photocatalytic performance, being one of the most promising technologies in environmental prevention and remediation [17–19]. Nevertheless, sensitization suffers from some important drawbacks. Some examples are the photostability of the charge-transfer sensitizers or the general difficulty in establishing stable surface anchorage to the titania surface to avoid leaching in liquid media.

So far, efforts in sensitization have been mostly directed to the post-synthetic surface modification of the titania, being the well known ruthenium bipyridyl complex [Ru(4,4′-H$_2$dcbpy)$_2$(SCN)$_2$] (N3 dye; 4,4′-H$_2$dcbpy = 4,4′-dicarboxy-2,2′-bipyridine; Fig. 1) one of the most widely studied and successful sensitizers [8,20]. Nevertheless, the development of new *in-situ* sensitizing synthetic methods based in co-condensation reactions is an actually unexplored field. This more eco-friendly strategy should led to the design of new hybrid materials with the functionality more closely integrated in the semiconductor matrix.

We have recently shown the successful low temperature incorporation of photoactive organic moieties in the crystal structure of titania, causing distortion in localized sites in the anatase network,

* Corresponding authors.
E-mail addresses: jesus.berenguer@unirioja.es (J.R. Berenguer), j.garcia@ua.es (J. García-Martínez).
[1] Homepage: www.nanomol.es.

by using a new one-pot co-condensation strategy, the so-called "Sol-Gel Coordination Chemistry" [21,22]. The hybrid organotitanias showed a very significant reduction of its band gap (up to 2.74 eV) and revealed highly active and remarkably stable photocatalytic properties.

Encouraged by these results and taking into account the charge transfer sensitizing properties of coordination complexes, we decide to explore the extension of this one-pot strategy to the incorporation of the neutral Ru(II) N3 dye and a new cationic Ir(III) compound ([Ir(ppy)$_2$(3,3′-H$_2$dcbpy)]PF$_6$) in the structure of titania (Fig. 1). This *in-situ* procedure produces hybrid titania-based photocatalysts (**TiO$_2$_Ru_IS** or **TiO$_2$_Ir_IS**), which present an exceptional stability. The synthesized materials were evaluated in liquid-solid regime for the degradation of the commercial R6G dye under UV and visible light irradiation.

2. Experimental

2.1. General methods

Complexes **1** and **2** have been characterized by elemental analyses, mass spectrometry and the usual spectroscopic means (IR, Vis/UV, multinuclear NMR) and its emissive properties have been studied on a Jobin-Yvon Horiba Fluorolog 3-11 Tau-3 spectrofluorimeter. The HOMO and the LUMO energies, corresponding to the ionization potential (IP) and the electron affinity (EA), respectively, have been estimated by cyclic voltammetry.

The incorporation of both coordination compounds in the titania samples was evaluated by DRUV, FTIR and XPS spectroscopy techniques, and the content of both organic compounds in the final titania materials was analyzed by elemental analysis. XRD analysis was carried out in order to study the crystalline structure of the titania materials and TEM was used to study their morphology, porosity and crystallinity. The particle size was calculated by TEM, using the software Gatan, being estimated as an average of the size of 100 particles. Porous texture parameters (mesoporosity volume, surface area and pore diameter) were characterized by N$_2$ adsorption at 77 K and the results were analyzed using the software package AUTOSORB. DRUV spectra were carried in order to determinate the band gap of the titania materials. XPS spectra of these materials were obtained in the −10 to 2 eV region to calculate the position of the maximum of their valence bands. Both techniques were combined to determine the maximum of the conduction band position of the titania materials and to obtain the density of states (DOS) scheme.

Photocatalytic activity of the synthesized materials was evaluated by photocatalytic degradation of Rhodamine 6G molecules in aqueous solution under UV or visible radiation. The samples irradiated with UV light were studied with a total organic carbon analyzer to determinate the TOC content of the synthesized samples before and after bleaching of the sample.

Full equipment and experimental conditions used and the crystallographic data of the monocrystal X-ray diffraction study of complex **2** are included in the ESI.

2.2. Synthesis of [Ru(4,4′-H$_2$dcbpy)$_2$(SCN)$_2$]·4H$_2$O (1)

This compound was synthesized as described before [20]. IR (KBr, cm^{-1}): ν(O—H) 3431 (s broad); ν(C—H) 3108 (s), 3065 (s), 2963 (s), 2923 (s); 2854 (s), ν(C=N) 2110 (*vs*), 1998 (m); ν (C=O) 1716 (*vs*); 1618 (m); 1550 (m); 1383 (m); 1261 (*vs*); ν(OC—O) 1230 (vs); 1019 (m); ν(C=S) 769 (s); 750 (m). ^{1}H NMR (δ, 300 MHz, CD$_3$OD, 25 °C, TMS) Broad signals with not well resolved multiplicity. 9.63 (s br, 2H, H^6), 9.09 (s, 2H, H^3), 8.93 (s, 2H, H$^{3'}$), 8.35 (s, 2H, H^5), 7.83 (d, ^3J(H,H) = 5.9 Hz, 2H, H$^{6'}$), 7.67 (d, ^3J(H,H) = 5.9 Hz, 2H, H$^{5'}$).

2.3. Synthesis of [Ir(ppy)$_2$(3,3′-H$_2$dcbpy)]PF$_6$ (2)

This compound was synthesized in a similar way to that previously described for the 4,4′-dcbpy isomer [23]. A yellow solution of 0.25 g (0.23 mmol) of [Ir(ppy)$_2$(μ-Cl)]$_2$ in 20 ml of CH$_2$Cl$_2$ was treated with a solution of 0.12 g (0.47 mmol) of 2,2′-bipyridin-3,3′-dicarboxylic acid (3,3′-H$_2$dcbpy) in 20 ml of MeOH, and the mixture was refluxed for 2 h. 5 ml of a saturated solution of NaAcO in MeOH was added to the above solution and the mixture was again refluxed during 1 h. Finally, 5 ml of a saturated solution of NH$_4$PF$_6$ in MeOH was added to the final mixture, stirring it for further 30 min. The resulting solution was evaporated to dryness and the solid residue was treated with 20 ml of HCl 1 M, stirring the mixture during 10 min at room temperature. The orange solid formed was filtered and washed with water (2 × 10 ml) and extracted with MeOH. 5 ml of a saturated solution of NH$_4$PF$_6$ in MeOH were added and the mixture was stirred for 30 min and evaporated to dryness. The residue was extracted with CH$_2$Cl$_2$ and the resulting solution was evaporated to dryness to give the compound **2** as an orange solid (0.19 g, 59%). Anal. Calcd. for C$_{34}$H$_{24}$F$_6$IrN$_4$O$_4$P: C, 45.90; H, 2.72; N, 6.30. Found: C, 46.30; H, 3.13; N, 5.96. ESI(+): 754.14 ([M-PF$_6$]$^+$, 100%). IR (KBr, cm^{-1}): ν(O—H) 3400 (s broad); ν(C—H) 3103 (s), 3060 (s), 3031 (s), 2960 (m), 2920 (m); 2850 (m); ν(C=O) 1712 (s); 1612 (*vs*); 1476 (s); 1413 (s); 1303 (s); ν(OC—O) 1219 (s); ν(P-F) 845 (s). ^{1}H NMR (δ, 400 MHz, CD$_3$COD): 8.32 (d, J_{H-H} = 7.1 Hz, 2H, H^6, dcbpy);

Fig. 1. Schematic view of the complexes [Ru(4,4′-H$_2$dcbpy)$_2$(SCN)$_2$] (**1**) and [Ir(ppy)$_2$(3,3′-H$_2$dcbpy)]PF$_6$ (**2**), showing the numbering scheme used in the NMR characterization (see Experimental).

8.26 (br, 2H, H^2, ppy); 8.06 (d, J_{H-H} = 8.1 Hz, 2H, H^5, ppy); 7.98 (d, J_{H-H} = 4.6 Hz, 2H, H^4, dcbpy); 7.83 (t, J_{H-H} = 7.8 Hz, 2H, H^4, ppy); 7.77 (d, J_{H-H} = 7.7 Hz, 2H, H^8, ppy); 7.36 (s br, 2H, H^5, dcbpy); 7.05 (t, J_{H-H} = 6.5 Hz, 2H, H^3, ppy); 6.99 (t, J_{H-H} = 7.5 Hz, 2H, H^9, ppy); 6.85 (t, J_{H-H} = 7.4 Hz, 2H, H^{10}, ppy), 6.24 (d, J_{H-H} = 7.5 Hz, 2H, H^{11}, ppy). ^{13}C NMR (δ, 101 MHz, CD$_3$OD): 168.8 (s, CO$_2$H); 168.6 (s, C^{12}, ppy); 158.1 (s, C^{2or3}, dcbpy); 150.8 (s, C^4, dcbpy and C^{11}, ppy); 149.8 (s, C^{10}, ppy); 145.3 (s, C^2, ppy); 139.8 (s, C^6, dcbpy); 139.6 (s, C^4, ppy); 132.9 (s, C^9, ppy); 131.5 (s, C^8, ppy); 127.7 (s, C^5, dcbpy); 125.9 (s, C^6, ppy); 124.4 (s, C^3, ppy); 123.6 (s, C^7, ppy); 120.8 (s, C^5, ppy). ^{19}F NMR (376.5 MHz, CD$_3$COD, δ) −74.8 (d, $^1J_{F-P}$ = 710 Hz). ^{31}P NMR (162.1 MHz, CD$_3$COD, δ) −144.5 (d, $^1J_{F-P}$ = 710 Hz).

2.4. Synthesis of the mesoporous complex-free control titania

Mesoporous titania was prepared, without the aid of surfactant, according to the procedure previously reported by us [21]. In a typical synthesis, 5 g (14.7 mmol) of TBOT (tetrabutyl orthotitanate) was dissolved in 35 ml of absolute ethanol, under magnetic stirring. Following, 123.5 g (6.86 mol) of water was added drop-wise, causing the precipitation of the solid. The molar ratio of the synthesis gel was 1TBOT: 41.3EtOH: 467H$_2$O. The mixture was then reacted at room temperature during 24 h under vigorous magnetic stirring, and heated at 80 °C for other 24 h. The obtained solid product was filtered, washed with water and acetone and dried in an oven at 100 °C during 8 h (1.06 g, 90%).

2.5. Synthesis of the in-situ hybrid mesoporous metal complex-titania (TiO$_2$_Ru_IS, TiO$_2$_Ir_IS)

The synthesis of the hybrid mesoporous titania-based materials **TiO$_2$_M_IS** (M = Ru, Ir) was carried out accomplishing the co-condensation of the titania precursor (TBOT) with the complexes **1** or **2**, also without the concurrence of surfactants. The details are proprietary [21,24]. A solution of the corresponding complex in 2 ml of absolute EtOH (0.04 g, 0.06 mmol **1**; 0.08 gr, 0.09 mmol **2**) was added to 5 g (14.7 mmol) of TBOT. The mixture was stirred during 30 min and then it was dissolved in 35 ml of absolute ethanol, under magnetic stirring. Following the same procedure described above for the control titania, the mesoporous hybrid metal complex-titania were obtained as pale garnet (**Ru**) or beige solids (**Ir**). **TiO$_2$_Ru_IS**: the molar ratio of the synthesis gel was 1TBOT: 4·10^{-3} Complex **1**: 41.3 EtOH: 467H$_2$O (0.97 g, 80%). IR (KBr, cm^{-1}): ν(O−H) 3400 (vs broad), 3065 (m), 3027 (m); ν(C−H) 2965 (w), 2925 (w), 2854 (w), 2831 (w); ν(C≡N) 2113 (w), 1997 (s); δ(O−H) 1620 (vs); ν_{as}(-COO) 1539 (m); 1429 (w); 1404 (w); ν_s(−COO) 1366 (m); 1234 (w); ν(Ti-O) 573 (vs broad), 474 (vs broad). **TiO$_2$_Ir_IS**: the molar ratio of the synthesis gel was 1TBOT: 6·10^{-3} Complex **2**: 41.3 EtOH: 467H$_2$O (1.20 g, 97%). IR (KBr, cm^{-1}): ν(O−H) 3400 (vs broad); ν(C−H) 2960 (w), 2921 (w), 2851 (w); δ(O−H) 1620 (vs); ν_{as}(−COO) 1477 (m), 1436 (w); 1417 (w); ν_s(-COO) 1381 (m); 1219 (w); 1156 (m); ν(Ti−O) 593 (vs broad); δ(Ti-O) 470 (vs broad).

2.6. Reaction of [Ir(ppy)$_2$(4,4′-dmbpy)](PF$_6$) with TBOT

In a similar way to that described for the preparation of the in-situ hybrid mesoporous metal complex-titanias **TiO$_2$_M_IS**, a solution of complex [Ir(ppy)$_2$(4,4′-dmbpy)](PF$_6$) (4,4′-dmbpy = 4,4′-di-methyl-2,2′-bipyridine) in 2 ml of absolute EtOH (0.05 g, 0.06 mmol) was added to 5 g (14.7 mmol) of TBOT. The mixture was stirred during 30 min and then it was dissolved in 35 ml of absolute ethanol, under magnetic stirring. Following, 123.5 g (6.86 mol) of water was added drop-wise, causing the precipitation of the solid. The mixture was then reacted at room temperature during 24 h under vigorous magnetic stirring, and heated at 80 °C for other

24 h. The obtained solid product was filtered, washed with water and acetone, yielding a yellow filtrate and a white solid, which was dried in an oven at 100 °C during 8 h (1.10 g, 93%). This white solid was characterized as complex-free titania.

2.7. Synthesis of the grafted mesoporous metal complex-titania (TiO$_2$_Ru_G, TiO$_2$_Ir_G)

The synthesis of the grafted titanias **TiO$_2$_M_G** (M = Ru, Ir) were carried out to obtain materials with similar Ti/metal complex molar ratio than those obtained in the hybrid in-situ metal complex-titanias. In a typical synthesis, 1.17 g of the synthesized complex-free control titania (14.65 mmol) were added to a solution of the corresponding complex in 35 ml of EtOH (0.04 g, 0.06 mmol **1**; 0.08 gr, 0.09 mmol **2**). The mixture was stirred during 30 min until a homogeneous distribution was provided. Then, the mixture was refluxed overnight. The obtained purple (**1**) or beige (**2**) solid was filtered off, washed with EtOH and acetone, and dried in an oven at 100 °C during 8 h. **TiO$_2$_Ru_G**: (0.95 g, 78%). IR (KBr, cm^{-1}): ν(O−H) 3420 (vs broad); ν(C−H) 2963 (w), 2924 (w), 2851 (w); ν(C≡N) 2114 (w), 1997 (w); δ(O−H) 1620 (s); ν_{as}(-COO) 1540 (m); 1433 (w); 1405 (w); ν_s(-COO) 1366 (m); 1263 (w); 1233 (w); ν(Ti-O) 570 (vs broad), 480 (vs broad). **TiO$_2$_Ir_G**: (0.85 g, 69%). IR (KBr, cm^{-1}): ν(O−H) 3412 (vs broad); ν(C−H) 2924 (w), 2848 (w); δ(O−H) 1620 (vs); ν_{as}(-COO) 1478 (m); 1436 (w); 1418 (w); ν_s(-COO) 1384 (m); 1220 (w); 1154 (m); ν(Ti-O) 593 (vs broad); δ(Ti-O) 470 (vs broad).

3. Results and discussion

3.1. Coordination precursors

[Ru(4,4′-H$_2$dcbpy)$_2$(SCN)$_2$]·4H$_2$O (**1**) was synthesized as described elsewhere (garnet solid) [20], while [Ir(ppy)$_2$(3,3′-H$_2$dcbpy)]PF$_6$ (**2**) (Hppy 2-phenylpyridine) has been obtained by reaction of [Ir(ppy)$_2$(μ-Cl)]$_2$ with 3,3′-H$_2$dcbpy, following a similar method to that previously described for the 4,4′-H$_2$dcbpy isomer [23]. Complex **1** and **2** have been fully characterized by analytical and spectroscopic means (see Experimental and ESI). Also, an X-ray diffraction study has been carried out on an orange monocrystal of complex **2**, obtained by cooling a saturated dichloromethane solution of the complex at −30 °C. As shown in Fig. 2a, the molecular structure of the cation **2$^+$**, [Ir(ppy)$_2$(3,3′-H$_2$dcbpy)]$^+$, presents the expected pseudooctahedral environment, with bond distances and angles (see ESI, Table S1) similar to those observed for the neutral monoprotonated iridium(III) complex [Ir(ppy)$_2$(4,4′-Hdcbpy)] and related derivatives [23,25,26]. As observed in other complexes containing the 3,3′-H$_2$dcbpy ligand [27,28], the steric repulsion between the carboxylic acid units on the bipy ligand is released by twisting the pyridine rings to a dihedral angle of 26.53°. This distortion favors the formation of hydrogen bonds (O−H···O) between the carboxylic acid groups, giving rise to the formation of dimers (Fig. 2b. O···O 2.6 Å, H···O 1.8 Å, O−H···O 169°) [29].

The DRUV spectrum of complex **1** (Fig. 3, Table 1. See also ESI, Fig. S2) shows two high energy bands (230, 322 nm) due to spin-allowed ligand centered ($\pi\pi*$) transitions localized on the H$_2$dcbpy ligands, and two intense low energy bands (408 nm, 540 nm), attributed to spin-allowed metal-to-ligand charge transfer (^{1}MLCT) [20], with a shoulder at 650 nm extending to 800 nm, which is associated with spin-forbidden ^{3}MLCT. The spectrum resembles to that described in ethanolic solution (314, 398 and 538 nm, see Table 1) [20]. It is worth to note that the absorption spectrum of this complex in solution depends on the nature on the solvent and the protonation of the carboxylate groups of the bipyridine ligand. Thus, the tetra anionic species (NBu$_4$)$_4$[Ru(4,4′-dcbpy)$_2$(SCN)$_2$] exhibit in ethanolic solution a remarkable blue shift

Table 1
Photophysical data for complexes **1** and **2** and the hybrid metal complex-titanias.

	Absorption data (298 K)		Emission data	
Sample	Media	λ_{abs}/nm (ε/M^{-1} L^{-1})	λ_{em}/nm (λ_{ex}/nm)	τ/μs [ϕ/%]
[Ru(4,4′-H₂dcbpy)₂(SCN)₂] (1)	EtOH[a]	314 (48.2), 398 (14.0), 538 (14.2)	At 298 K, 830(310)	0.02 [0.04]
	Solid	230, 322, 408, 540, 650(sh)		
(NBu₄)₄[Ru(4,4′-dcbpy)₂(SCN)₂]	EtOH[a]	308 (45.9), 380 (13.3), 518 (13.0)		
TiO₂_Ru_IS	Solid	280, 390sh, 500 (extending to 700 nm)		
TiO₂_Ru_G	Solid	280, 390sh, 504 (extending to 700 nm)		
[Ir(ppy)₂(3,3′-H₂dcbpy)]PF₆ (2)	CH₂Cl₂[b]	257 (28.8), 289sh (19.9), 381 (4.2), 407 (3.0), 512[c] (0.4)		
	MeOH[b]	254 (28.9), 287sh (17.4), 381 (3.5), 401 (2.7), 470[d] (0.3)		
	MeCN[b]	253 (30.0), 289sh (19.8), 381 (5.0), 403 (3.6), 475 (0.6), 514sh (0.5)	At 298 K, 625(425) At 77 K, 600(450)	
	Solid	290, 320, 380, 470, 510	At 298 K, 648(400) At 77 K, 624(400)	0.03 [4]
TiO₂_Ir_IS	Solid	280, 316, 380, 470 (extending to 540 nm)		
TiO₂_Ir_G	Solid	280, 316, 380, 470 (extending to 540 nm)		

[a] Solutions 1×10^5 M. Data from reference [7].
[b] Solutions $5*10^{-5}$ M.
[c] Tail extending to 570 nm.
[d] Tail extending to 530 nm.

Fig. 2. a) Molecular structure of the complex cation [Ir(ppy)₂(3,3′-H₂dcbpy)]⁺ (**2⁺**). Most relevant bond lengths (Å): Ir-C 2.011(3), 2.015(3). Ir-N(ppy) 2.043(3), 2.048(3). Ir-N(bpy) 2.138(3), 2.155(3). b) View of the molecular dimer formed by the existence of hydrogen contacts (O—H···O) between the carboxylic acid groups.

Fig. 3. Solid state DRUV spectra of the complexes [Ru(4,4′-H₂dcbpy)₂(SCN)₂] (**1**) and [Ir(ppy)₂(3,3′-H₂dcbpy)](PF₆)(**2**), and those of their corresponding hybrid metal complex-titanias as compared with the control TiO₂.

in the absorption maxima (308, 380, 518 nm) and, in aqueous solution, the low energy feature of complex **1** is found at 500 nm at pH 11 and at 520 nm at pH 1 [20]. The observed blue-shift has been ascribed to an increase in the energy of the LUMO, mainly located on the dcbpy ligands, causing the $\pi\pi*$ and dπ-$\pi*$ transitions to occur at higher energies.

The DRUV spectrum of complex **2** (Fig. 3 and S2) shows two high energy bands at 290 and 320 nm, assigned to allowed $\pi\pi*$ transitions associated to the H₂dcbpy and the ppy groups. At lower energies, complex **2** shows an intense absorption at 380 nm, attributed, with reference to similar complexes [23,25], to a mixture of spin allowed ^{1}MLCT and ligand-to-ligand charge transfer
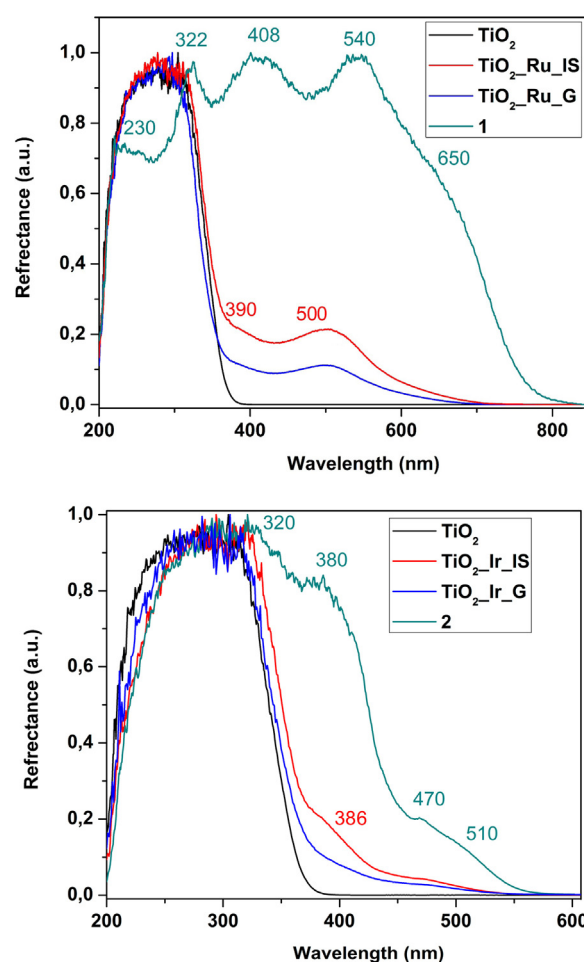
transitions (^{1}LL'CT). The weak feature at 470 nm, extending to 570 nm, which is also observed in solution, is assigned to a mixture of spin-forbidden ^{3}MLCT [dπ(Ir) → $\pi*_N$Û$_N$], ^{3}LL'CT [$\pi_{C^\wedge N}$ → $\pi*_{N^\wedge N}$] and ^{3}LC (ppy) transitions [23,25]. The absorption maxima observed in solution (253, 289sh, 381, 403, 475, 514sh nm in MeCN) are close to those observed in the solid state. Only a minor hypsochromic

shift is observed for the lowest energy feature in polar solvents (Table 1 and Fig. S3).

As reported elsewhere [20], complex **1** shows a very weak emission band centered at 813 nm (τ 30 ns; ϕ 0.0004) in ethanol, derived from a ^{3}MLCT excited state. The cyclometalated Ir(III) complex **2** is highly emissive both in solution and in solid state (Table 1). In the solid state at 298 K, complex **2** shows a broad and feature-less phosphorescence (τ 30 ns) centered at 648 nm with a quantum yield of $\sim$ 4%. The emission is blue-shifted at low temperature (624 nm), what is consistent with a typical charge transfer ^{3}MLCT [$d\pi$(Ir) $\rightarrow \pi^*_N{}^\wedge{}_N$] character of the emission [23]. In dilute acetonitrile, the emission profile shows an unstructured band peaking at 625 nm, being similar to that reported for the isomer with the 4,4′-H$_2$dcbpy ligand in the same solvent ([Ir(ppy)$_2$(4,4′-H$_2$dcbpy)]PF$_6$, 624 nm at 298 K, 576 nm at 77 K). However, in the frozen glass state, the emission is bathochromically shifted with respect to that of 4,4′-H$_2$dcbpy isomer (600 nm **2** vs 576 nm 77 K). This fact could tentatively be attributed to the formation of dimers through hydrogen bonding, which stabilizes the targed π^* orbital of the dicarboxylic-bpy ligand, decreasing the energy of the emission.

The HOMO and LUMO energies (vs vacuum) of the Ru(II) complex **1** have been previously described (HOMO -4.98 eV, LUMO -2.88 eV) [30], while the corresponding values for the Ir(III) complex **2** have been determined using cyclic voltammetry in CH$_2$Cl$_2$ solution (see ESI, General Methods and Fig. S4. HOMO -5.55 eV, LUMO -3.31 eV). The value of the HOMO-LUMO band gap (2.25 eV) calculated by electrochemical methods is similar to that obtained by absorption spectroscopy (2.14 eV) in solid state (DRUV) or solution (10^{-4} M, CH$_2$Cl$_2$).

3.2. Titania-based materials

The synthesis of the hybrid titania-based materials (**TiO$_2$_M_IS**) is depicted in Scheme 1 (for more details see Experimental). By mixing an ethanolic solution of complexes **1** and **2** with TBOT (metal complex/TBOT $\sim$ 0.005 molar ratio) pale-coloured solutions were obtained, which contain polymetallic Ru(II)- or Ir(III)-titanium alkoxide intermediates homogeneously dispersed (i, Scheme 1). These intermediates are proposed to be mainly made of dititanium units through bidentate bridging carboxylate groups, with a bonding situation similar to that previously described elsewhere [20,31], although monodentate or chelating bidentate coordination to titanium centers are also likely in some extent. Due to the flexibility of the medium, all carboxylate groups (four in **1** and two in **2**) are probably involved in bonding. Room temperature hydrolysis of these mixtures by vigorous stirring (24 h, ii, Scheme 1) afforded a gel, which crystallizes adopting an anatase phase after heating (80 °C) the suspensions for 24 h (iii, Scheme 1). After the filtering and the washing of the samples, garnet (**TiO$_2$_Ru_IS**) or beige (**TiO$_2$_Ir_IS**) mesoporous materials were obtained. For comparison purposes, a metal-free control TiO$_2$ was prepared following the same experimental procedure. In addition, two related conventional grafted titania materials (**TiO$_2$_Ru_G** or **TiO$_2$_Ir_G**) have also been prepared starting from the aforementioned control TiO$_2$, and using a similar Ti/metal complex molar ratio than that employed for the hybrid in-situ metal complex-titanias (see Experimental).

The importance of the carboxylate groups of the bpy ligand in the formation of the hybrid in-situ titania materials under the conditions outlined above was assessed by using [Ir(ppy)$_2$(4,4′-dmbpy)](PF$_6$) (4,4′-dmbpy = 4,4′-di-methyl-2,2′-bipyridine) [32], which presents a similar molecular size that complex **2**, as coordination dye. In this case no incorporation to the titania material was observed, and only metal-free control titania was obtained (see Experimental). This fact excludes the possibility of superficial adsorption or, indeed, occlusion of the dye in the titania
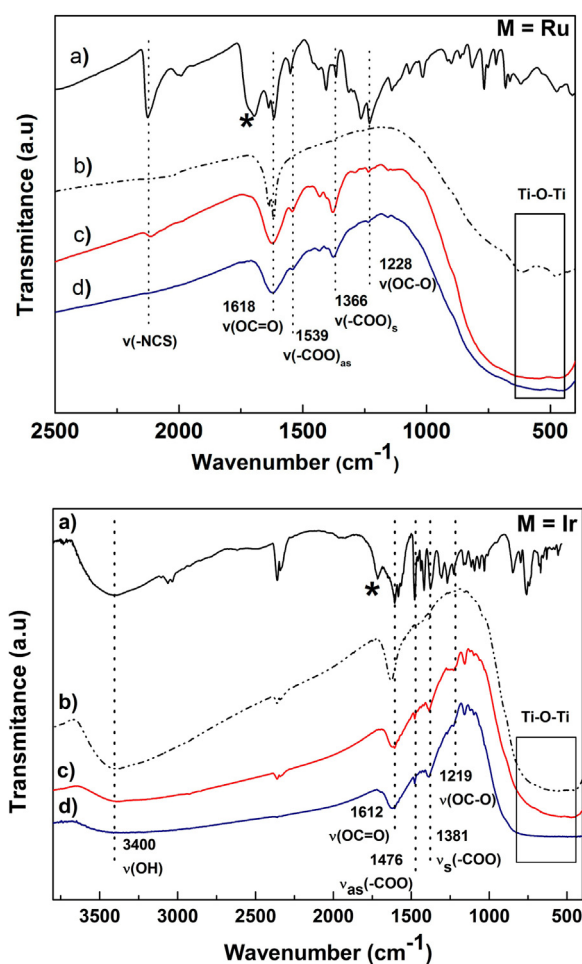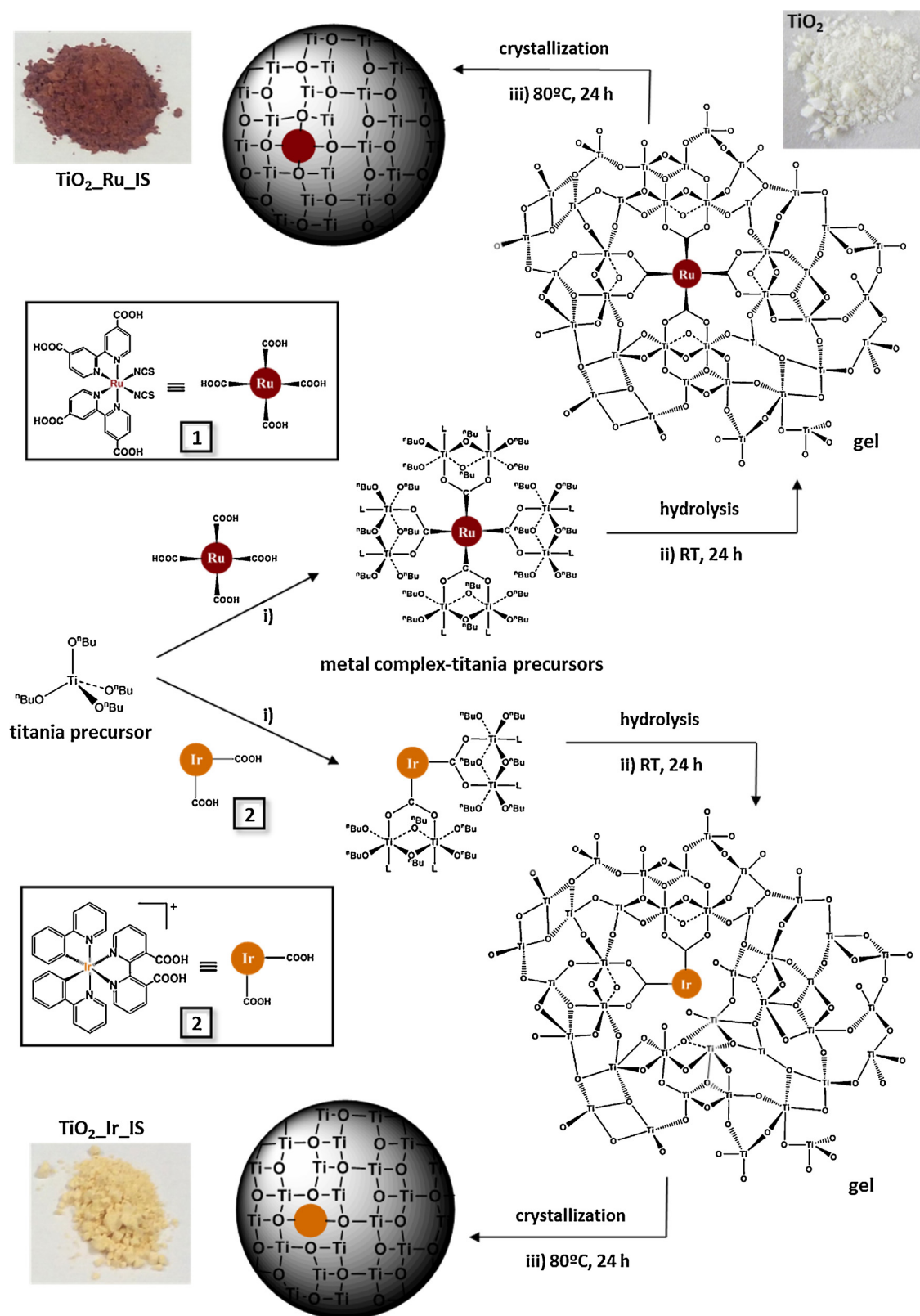

Fig. 4. FTIR spectra of the ruthenium- (up) or iridium- (down) titania materials **TiO$_2$_M_IS** (c) and **TiO$_2$_M_G** (d) in comparison with the spectra of the pure complexes **1** and **2** (a) and the control TiO$_2$ (b). (*) ν(OC=O) of the terminal –COOH groups.

nanoparticles without the aid of a bonding interaction between the coordination dye and the semiconductor network.

As shown in Fig. 3, the DRUV spectra (see also Table 1) clearly determine the incorporation of the corresponding metallic complexes (**1**, **2**) in both types of materials (**TiO$_2$_M_IS** or **TiO$_2$_M_G**; M = Ru, Ir). The most significant bands are the two low energy absorptions (a shoulder at 390 nm and a band at ca. 500 nm for M = Ru; 380 and 470 nm for M = Ir) in the visible region. These features are close to that described for complexes **1** and **2**, respectively, both in solution and in solid state. The DRUV spectra also suggest a higher incorporation of the coordination dyes for the hybrid in-situ materials than for the grafted ones, a fact which has also been confirmed by ICP analyses, indicating the effectiveness of the synthetic method herein described. Thus, the metal complex incorporation for the in-situ materials was ca. 92 wt% for **1** and 59 wt% for **2**, while the values obtained for the related grafted materials **TiO$_2$_M_G** were lower (60 wt% for **1** and 23 wt% for **2**. ICP, see Table 2). The lower incorporation for the Ir(III) dye **2** in both types of materials, might be attributed to its fewer number of carboxylate groups and its cationic nature.

These materials have been also characterized by FTIR and XPS. The FTIR spectra of the complexes **1** and **2** and all the titania samples (including the metal-free control titania) are shown in Fig. 4. As expected, the FTIR spectra of both metal complex-titania materials (**IS** and **G**) show distinctive bands of the corresponding pure complexes. A broad band at 3400 cm^{-1}, characteristic of associ-

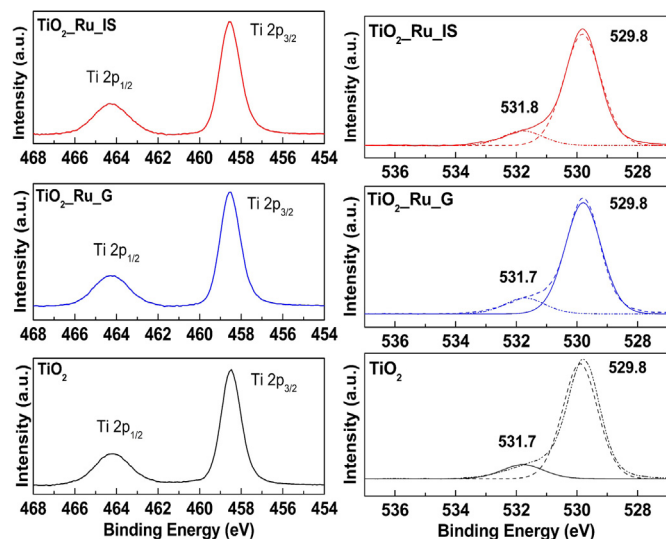Scheme 1. Synthesis of the hybrid metal complex-titania **TiO₂_Ru_IS** and **TiO₂_Ir_IS** materials.

ated hydroxyl groups, overlaps with the C−H stretching vibrations of the heteroaromatic pyridines expected about $3100 \, cm^{-1}$ [33]. For **TiO₂_Ru_IS**, a band corresponding to the thiocyanate ligand is observed at $2113 \, cm^{-1}$ [33]. All the materials are characterized by the disappearance of the $\nu(OC=O)$ stretching mode of the terminal

COOH groups ($1716 \, cm^{-1}$ **1**; $1712 \, cm^{-1}$ **2**), suggesting the incorporation of the dyes through the binding of the carboxylate groups with the titania precursor [34,35]. As expected, the vibrations typically associated to the bridging bidentate groups ($\sim 1370 \, cm^{-1}$ for $\nu_s(-COO)$; $\sim 1500 \, cm^{-1}$ for $\nu_{as}(-COO)$) are observed in both,

Table 2
Textural and structural parameters of the hybrid metal complex-titanias as compared to the control titania.

Sample	M[a] (wt%)	M[a] (mol%)	Inc. yield[a] (%)	d_p[b] (nm)	V_p[c] (cm^3/g)	A_{BET}[d] (m^2/g)	$D^{XRD,e}$ (nm)	$d_{101}^{XRD,f}$ (nm)	$d_{101}^{TEM,g}$ (nm)
TiO₂	–	–		5.6 (2–9)	0.29	245	6.4	0.35	0.37
TiO₂_Ru_IS	0.49 (0.53)	0.35 (0.38)	92	6.0 (3–11)	0.31	200	6.4	0.35	0.38
TiO₂_Ru_G	0.32 (0.53)	0.24 (0.38)	60	6.0 (3–11)	0.35	240	6.1	0.35	0.38
TiO₂_Ir_IS	0.87 (1.47)	0.35 (0.59)	59	5.6 (1–9)	0.22	230	5.6	0.35	0.35
TiO₂_Ir_G	0.34 (1.47)	0.14 (0.59)	23	6.0 (2–12)	0.28	220	6.5	0.35	0.38

[a] Metal content calculated by ICP-OES analysis (see ESI). Values in brackets represent the theoretical values.
[b] Average mesopore diameters from N_2 isotherm.
[c] Mesopore volume from N_2 isotherm.
[d] BET surface area from N_2 isotherm.
[e] Crystalline domain size (calculated from XRD).
[f] Anatase spacing (d_{101}) from XRD.
[g] Anatase spacing (d_{101}) from TEM. See ESI for details.

Fig. 5. XPS spectra in the Ti 2p (left) and O 1s (right) regions of the **TiO₂_Ru_IS** and **TiO₂_Ru_G** materials as compared with the control TiO₂.

the grafted and the hybrid *in-situ* materials, being the intensity of these bands slightly more intense in the hybrid titanias. The broad band around 1610 cm⁻¹, which overlaps with the binding vibration of H—O bond from terminal groups in the TiO₂ [36], can be associated to the ν(OC=O) of monodentate carboxylate groups. In accordance, weak peaks at 1220 cm⁻¹, associated with ν(OC—O) stretching vibrations, are also observed in both hybrid materials.

XPS spectra of the hybrid titania samples and the control TiO₂ are shown in Fig. 5 (**Ru**) and S5 (**Ir**, see ESI). In both cases, the spectra in the Ti2p region of the control TiO₂ shows two signals at around 458.5 eV and 464.5 eV (Fig. 5 or S5, left), typical of Ti(IV) 2p₃/₂ and Ti(IV) 2p₁/₂ states, respectively, where Ti is in an octahedral coordination [15,37]. The O 1s XPS spectra (Fig. 5 or S5, right) of all the samples were deconvoluted using symmetric Gaussian curves. For the control TiO₂, the characteristic main peak at 529.8 eV is attributed to the oxygen in the metal oxide (Ti—O—Ti bonds) [38–41], while the additional one at 531.7 eV is related to the oxygen in a surface hydroxyl (Ti—OH species) and in carboxylic groups [7,38–43]. Both the grafted and the hybrid materials present their O 1s peaks at similar binding energies. The presence of Ru(II) or Ir(III) cannot be clearly observed in the XPS spectra due to the small amount incorporated (0.35 mol%) and the overlapping of their characteristic binding energies with other intense peaks (Ru 3p with Ti 2p at ∼460 eV, Ru 3d₃/₂ with one of the C 1s peaks at 287.8 eV, Ir 4f₅/₂ and Ir 4f₇/₂ with Ti 3 s at 62 eV) [15,42,44–46].

Fig. 6(a,b) presents the Tauc plots for **TiO₂_M_IS** and **TiO₂_M_G**, showing in all cases two different absorption band edges. The low energy absorption band edge is associated to the presence of the

Table 3
Constant values of the photocatalytic activity, regression coefficients and conversions at different times of the titanias with the complexes **1** and **2** as compared with the complex-free titania, TiO₂.

Samples	E_g[a] (eV)	k'*10³[b] (min⁻¹)	R[c]	%Conversion[d]			k'/k'$_{TiO2}$[e]
				1 h	2 h	3 h	
UV							
TiO₂	3.24	3.5 ± 1.0 (4.4)	0.9928	14.0	33.0	50.3	--
TiO₂_Ru_IS	2.82	19.5 ± 2.0 (20.3)	0.9935	61.2	88.6	96.8	5.6
TiO₂_Ru_G	3.00	6.0 ± 1.5 (7.5)	0.9781	39.2	64.1	71.1	1.7
TiO₂_Ir_IS	3.00	31.6 ± 1.0 (32.1)	0.9825	73.1	97.8	99.6	9.0
TiO₂_Ir_G	3.10	17.8 ± 0.8 (18.0)	0.9821	63.4	88.6	96.9	5.1
VIS							
TiO₂	3.24	2.5 ± 0.7 (2.63)	0.9640	20.2	31.7	39.0	–
TiO₂_Ru_IS	2.82	6.0 ± 0.4 (5.8)	0.9898	26.8	48.3	63.5	2.4
TiO₂_Ru_G	3.00	4.8 ± 0.3 (4.7)	0.9881	26.2	44.3	58.0	1.9
TiO₂_Ir_IS	3.00	18.2 ± 0.2 (18.0)	0.9697	86.2	90.9	97.3	7.3
TiO₂_Ir_G	3.10	9.3 ± 0.7 (9.5)	0.9973	44.7	67.40	82.7	3.7

[a] Band gap energies calculated from the intercept of the tangent to the $(F(R')h\nu^{1/2}$ versus ($h\nu$) plot.
[b] 1st order reaction rate pseudophotocatalytic constant of the reaction of degradation of an aqueous solution of Rhodamine 6 G (5 * 10⁵ M) obtained as the average of a minimum of three runs. Values in brackets indicate the k value used for the determination of the degree of conversion.
[c] Regression coefficient for the same degradation reaction as paragraph (b).
[d] Degree of conversion (%) achieved by the samples after 1 h, 2 h and 3 h of reaction.
[e] Ratio between the average k' values of the hybrid metal complex-titania materials as compared to the average k' value determined from the control TiO₂.

coordination dyes in the materials (eV/nm 1.70/729, Ru; 2.15/590, Ir), while the higher energy one is related to the indirect transitions of the anatase phase. Interestingly, in both of the *in-situ* hybrid materials (**TiO₂_M_IS**), the energy of this latest absorption band edge decreases with respect to that observed for the metal-complex free titania (3.24 eV) [21], causing a narrowing in their corresponding band gaps, which lie now in the visible region (Fig. 6d). Nevertheless, while the decrease in the indirect band gap transition is only of 0.24 eV for **TiO₂_Ir_IS** (3.00 eV, 413 nm), the energy is remarkably red-shifted for **TiO₂_Ru_IS** (2.82 eV, 440 nm). A similar behavior was observed in the formation of hybrid organotitanias, derived from the *in-situ* co-condensation of the TBOT with 4,6-dihydroxypirimidine and *p*-phenylenediamine [21]. The VB XPS spectra of both the hybrid **TiO₂_M_IS** also show a slight increase in the valence band maximum energy (VB maximum) of ca. 0.30 eV respect to that observed for the control titania (VB maximum at *ca.* 2.28 eV with the CB minimum at ca. −0.96 eV. Fig. 6c,d) [7,21].

It is worth noting that, although a similar behavior is also observed in the grafted titania materials (**TiO₂_M_G**), both effects are less pronounced. In the grafted materials the narrowing of the band gap is about half of that observed in the *in-situ* materials, with an increase of the energy of the VB maxima of ca 0.17 eV (Table 3, see ESI Fig. S6).
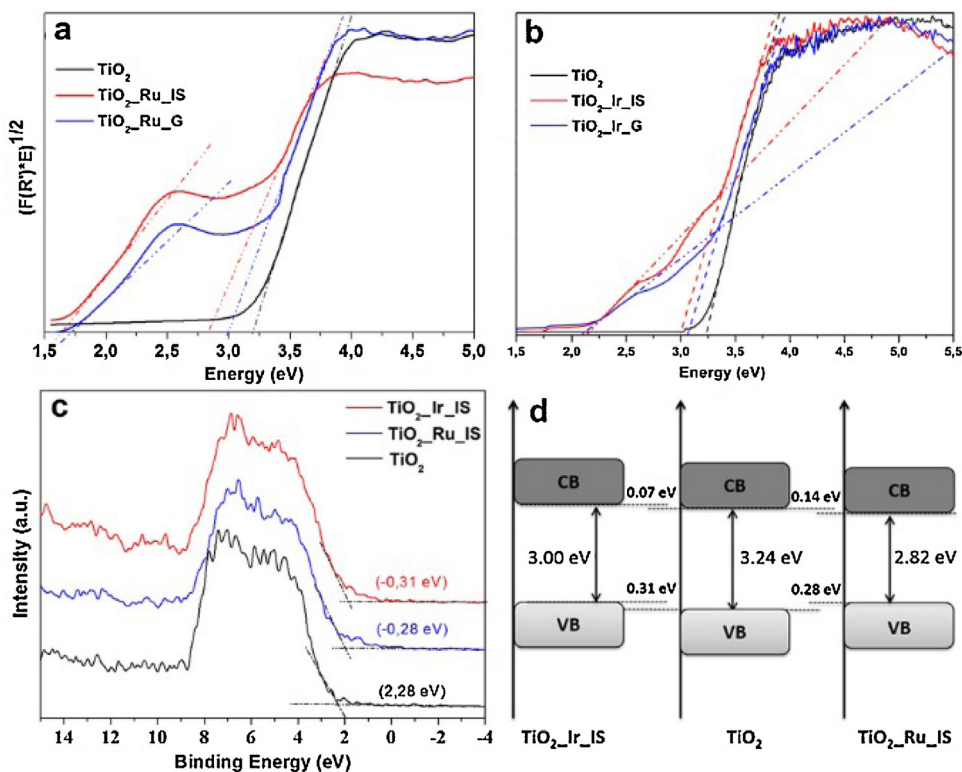
Fig. 6. Tauc plot of the transformed Kubelka-Munk function versus the energy of the light absorbed for the control titania and the titania-based materials containing the Ru(II) (a) and Ir(III) complexes (b). Valence band XPS spectra (c) and schematic illustration of the DOS (d) of the hybrid metal complex-titania **TiO₂_M_IS** (M = Ru, Ir) as compared with the control TiO₂.

Fig. 7. Representative nitrogen adsorption isotherms (left) and XRD patterns (right) of the hybrid *in-situ* materials **TiO₂_M_IS** (M = Ru, Ir) and the control TiO₂.

All the materials (**TiO₂_M_IS** and **TiO₂_M_G**) show Type IV isotherms and textural properties similar to those observed for the control TiO₂ (Table 2 and Fig. 7 left for **TiO₂_M_IS**; see ESI, Fig. S7 for **TiO₂_M_G**), indicative of the mesoporous nature of these samples. This mesoporosity is due to the interparticle void space between the small titania crystallites. As the grafted materials (**TiO₂_M_G**), both of the *in-situ* hybrid materials (**TiO₂_M_IS**) show high surface areas (200–230 m^{2}g^{-1}) and similar pore size between particles of *ca.* 6 nm, thus proving the effectiveness of the synthetic route herein proposed and the accessibility to reactive sites of these materials for photocatalytic applications. The XRD patterns of all titania materials (Fig. 7 right and ESI, Fig. S7) are characteristic of the anatase phase (2θ = 25.3°, 37.8° and 48.05°) [47], with the broad XRD peaks indicating that the materials synthesized are nanoparticles. All the materials (**TiO₂_M_IS** and **TiO₂_M_G**) display a crystalline domain

size of *ca.* 6 nm, very similar to that observed for the control TiO₂ (6.4 nm). Nevertheless, and despite the analogous size of both coordination complexes (a diameter of about 1.3 nm for **1** and 1.1 nm for the cation **2⁺**), the hybrid **TiO₂_Ir_IS** shows the lowest value of 5.6 nm.

The TEM analysis of the samples also confirms the interparticle mesoporous nature, formed by grains with a particle size of 7–9 nm, and the crystalline structure of all the titanias (Fig. 8). The d$_{101}$ lattice spacing, determined using the Gatan software on the TEM micrographs (Table 2), was 0.35–0.38 nm, which is similar to the spacing calculated by XRD (0.35 nm). This observation, and the similarity between the crystalline domain size determined by XRD and the average particle size calculated by TEM in all the samples (*ca.* 6 nm *vs. ca.* 8 nm), evidence that all materials, despite their small size of particle, have a high degree of crystallinity.
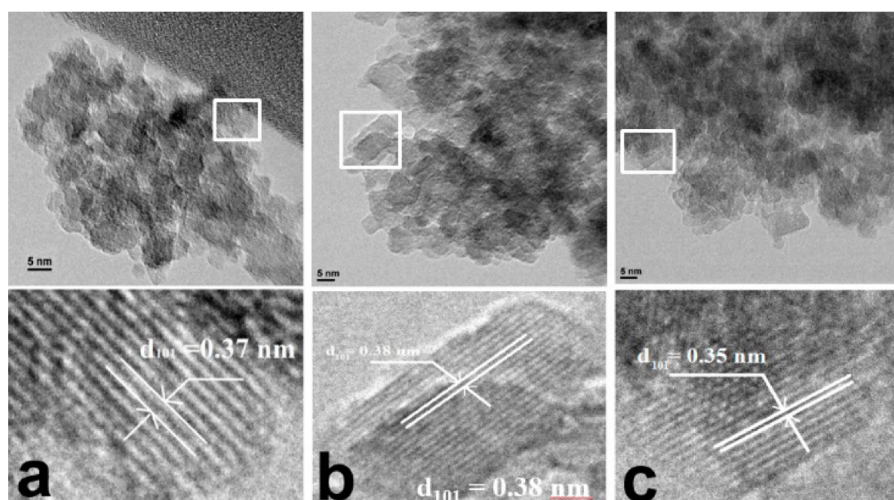
Fig. 8. Representative TEM micrographs of: a) control TiO_2, b) **TiO_2_Ru_IS** and c) **TiO_2_Ir_IS** materials.

Thus, as already outlined, although both types materials (**TiO_2_M_IS** and **TiO_2_M_G**) present anatase structure and similar textural and spectroscopic properties, the ICP analyses and DRUV spectra clearly show a more efficient uptake of the coordination dyes in the *in-situ* **TiO_2_M_IS**. Moreover, the narrowing of the primary band gap in relation to control TiO_2, determined by Tauc plots and Valence Band XPS spectra, is also more pronounced for the **TiO_2_M_IS**.

We also decide to investigate the differences in the stability of the coordination dyes in both types of materials by stirring them in aqueous 10^{-5} M NaOH solutions for different periods of times. The amount of the remaining dye after the basic washing was estimated based on the maximum absorbance (DRUV) at ca. 500 or 470 nm for the Ru(II)- or Ir(II)-titania-based materials, respectively (see ESI, Fig. S8). After one hour of stirring, the hybrid **TiO_2_Ru_IS** retains about 75% of the amount of the coordination dye, while the quantity has been reduced to the 50% in the grafted **TiO_2_Ru_G**. More impressive is the case of the hybrid **TiO_2_Ir_IS**, which retains about the 40% of the initial amount of the dye after one hour of stirring, while the grafted **TiO_2_Ir_G** maintains only a 10% of the dye after 2 min of stirring. Therefore, and compared with the standard post-synthetic grafting method (**TiO_2_M_G**), our *in-situ* synthetic approach led to the obtaining of hybrid **TiO_2_M_IS** materials with a higher uptake

of coordination dyes, which are actually better protected, probably due to a more efficient integration in the semiconductor matrix.

In both materials (**TiO_2_M_IS** and **TiO_2_M_G**) there must be dye incorporated on the surface of the titania. Nevertheless, during the formation of the hybrid **TiO_2_M_IS** materials, the dyes are homogeneously distributed in the precursor gel. After the crystallization step (iii, Scheme 1) part of them could be included in a network of amorphous titania coexisting with the anatase phase (although no amorphous titania in the final materials has been observed) or most likely introduced in the bulk as defects of the crystalline structure. This latter description of the materials is consistent with what we previously reported regarding the inclusion of organic fragments as crystal disruptors in the structure of visible active organotitanias [21].

3.3. Photocatalytic activity

Next, the photocatalytic activity of both of the *in-situ* hybrid and the grafted materials was tested by following the degradation of Rhodamine 6G (R6G) aqueous solutions under both UV and visible light irradiation. As detailed in Table 3 (see also Fig. 9 and ESI, Fig. S9), the *in-situ* hybrid materials **TiO_2_M_IS** (M = Ru, Ir) present a clear enhancement in their photocatalytic activity as com-
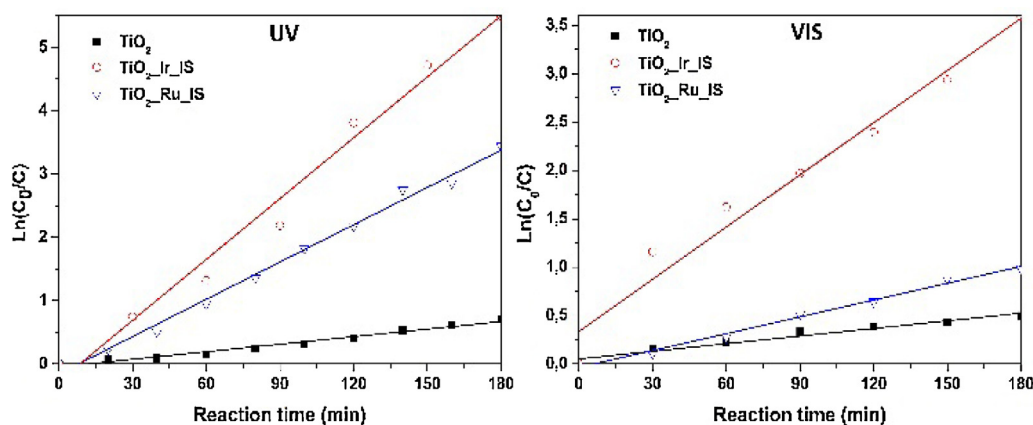

Fig. 9. Representation of the pseudophotocatalytic constant (k') of the **TiO_2_M_IS** (M = Ru, Ir) as compared with the control TiO_2, in the degradation reaction of an aqueous solution of rhodamine 6G ($5*10^{-5}$ M) under **UV** (left) or **visible** (right) irradiation.
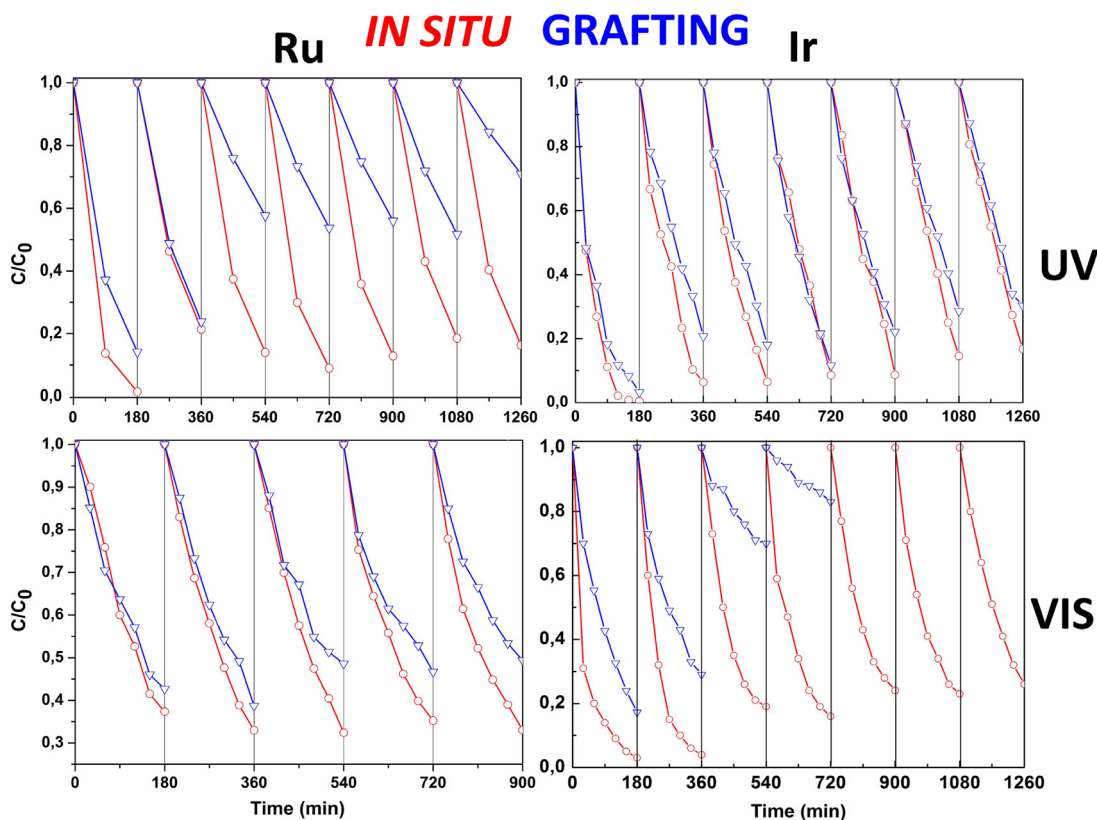
Fig. 10. Recycling tests of the degradation reaction of aqueous solutions of rhodamine 6 G ($5*10^{-5}$ M), carried out following the same conditions under **UV** (up) or **visible** (down) irradiation, of the *in-situ* **TiO$_2$_M_IS** (red circles) and the grafted **TiO$_2$_M_G** (blue triangles) titania-based materials (M = Ru, left; Ir, right).

pared to both the control titania (Table 3) and the grafted materials **TiO$_2$_M_G** (k'$_{IS}$/k'$_G$ = 3.3 Ru, 1.8 Ir, UV; 1.2 Ru, 2.0 Ir, VIS). In particular, the photocatalytic activity of **TiO$_2$_Ir_IS**, which presents the lowest crystalline domain size (5.6 nm), is much higher than not only that of the control titania (up to nine- or seven-fold under UV irradiation or visible light, respectively Table 3), but also than of the Ru(II) material **TiO$_2$_Ru_IS** (up to three-fold under visible light). Notwithstanding, the improvement in the photocatalytic activity for both the *in-situ* materials could be attributed to the synergic combination of the band gap reduction and the higher concentration of dye with respect to the grafted ones.

As shown in Fig. 10, the recycling tests carried out under both UV and visible irradiation, reveal that the **TiO$_2$_M_IS** also exhibits greater stability than the **TiO$_2$_M_G**. All the *in-situ* hybrid materials retain, after seven photodegradation cycles, more than 75% of its corresponding efficiency (100% in the case of **TiO$_2$_Ru_IS** under visible irradiation). The stability of **TiO$_2$_Ir_IS** under visible irradiation (75% after seven cycles) is particularly remarkable, as the activity of its counterpart **TiO$_2$_Ir_G** falls below 20% only after 4 cycles. To confirm the higher stability of the incorporated dyes in the *in-situ* materials, not only against leaching but also under photodegradation conditions, both titania-based materials were stirred under illumination for 9 h (equivalent to three recycling cycles), simulating the situations in which the loss of the efficiency of the grafted materials is more evident (**TiO$_2$_Ru_G** under UV irradiation and **TiO$_2$_Ir_G** under visible light). This study revealed that after irradiation, the *in-situ* materials retain about 40% of the dye, while the amount of the dye in the grafted materials is lesser than the 15% (see ESI, Fig. S10), thus again indicating that the better integration of the dye in the semiconductor matrix provides an exceptional stability to the final *in-situ* materials.

Regarding the photocatalytic mechanism, it is worth noting that, as aforementioned, the **TiO$_2$_M_IS** materials present reduced band gaps (M = Ru 2.82 eV, Ir 3.00 eV) and, therefore, they should be able to be excited not only by UV light irradiation but also by the visible light, producing reactive hole-electron pairs (*the hole way*), which finally give rise to the formation of the ·OH radicals responsible of the degradation of the organics (Fig. 11) [21,48]. Simultaneously, the semiconductor is also sensitized by the coordination dye, which is able to absorb between 200 and 500 nm (or even 600 nm in the case of **1**). Absorption of light induces the excitation of the dye and triggers the subsequent electron transfer to the conduction band of the semiconductor (*the dye way*, Fig. 11. See also Fig. S4 in ESI for the energy levels).

To gain a better understanding of the degree of the contribution of each mechanism to the total activity of the hybrid materials, the influence of two different scavengers in the photodegradation process under UV or visible light irradiation was examined (see ESI, Table S3) [49]. It has been observed that both the addition of isopropanol, as a hydroxyl radical scavenger, and, specially, the addition of triethanolamine, as a hole scavenger, only cause moderate variations in the photodegradation rate. This result agrees with the fact that, at least in the experimental conditions used, although both mechanisms (*the dye and the hole way*) should be active, *the dye way* seems to be the dominant mechanism, even under UV irradiation. This fact contrasts to the preponderance of *the hole way* observed under visible light for the previously reported black organotitania **TiO$_2$-PPD**, under the same reaction conditions [21].

We also note that the mechanism of degradation of the R6 G seems to be influenced by the type of illumination (UV or visible light) as suggested by controlling its characteristic band at 525 nm during the photocatalysis (Fig. 12. See also ESI, Figs. S11–14). The
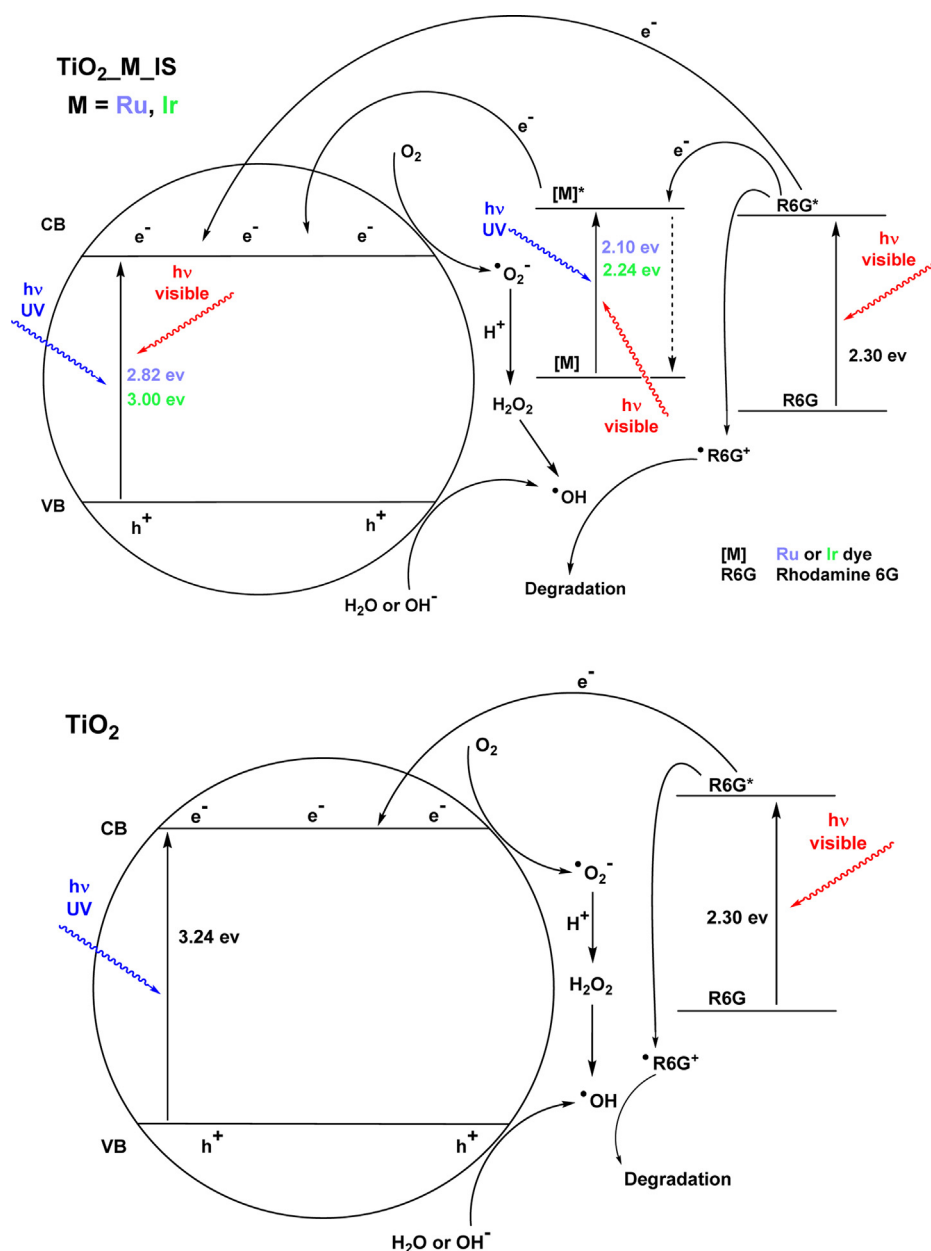
Fig. 11. Schematic representation of the photo-induced charge transfers in the bare **TiO$_2$** and the **TiO$_2$_M_IS** system and the mechanism of the photocatalytic degradation process (energetic values in violet for **TiO$_2$_Ru_IS**, 2.82 eV and 2.10 eV, and green for **TiO$_2$_Ir_IS**, 3.00 eV and 2.24 eV).

measurements carried out for the control TiO$_2$ reveal a systematic blue-shift from 525 nm to 515 nm under both types of light. This behavior has been previously associated with a selective N-deethylation of R6G to rhodamine previous to the destruction of the polyaromatic system [50]. This fact indicates that the ˙OH radicals attack primarily the R6G areas that connect directly with the surface of the titania, inducing the photocatalytic degradation of the R6G on the surface of the photocatalyst [50,51]. It should be noted that control TiO$_2$ is able to photodegradate R6G under visible light acting only as an electron mediator between the excitation of the R6G (2.23 eV) and the formation of the ˙OH radicals (Fig. 11) [21].

By contrast, in both cases, the hybrid and grafted materials, a blue-shift of the maxima at 525 nm is clearly observed only under visible light (to 510 nm for Ru(II) or 500 nm for Ir(III). See ESI, Figs. S11–S12). Nevertheless, under UV illumination the band at 525 nm decreases without shift (see ESI, Figs. S13–S14), suggesting that the

R6 G degradation occurs in the bulk by initial cleavage of the polyaromatic dye system, giving rise, firstly, to organic species which does not contain aromatic rings [52]. Accordingly, TOC measurements carried out on the solutions before and after their irradiation with UV light in the presence of the catalysts indicated only a partial degradation of the total organic dissolved carbon (up to ca. 50%) when the total dye bleaching was reached (ca. 3 h). This indicates that, although no R6G is left in the reaction mixture, there are still non-aromatic carbon species, such as aldehydes and/or carboxylic acids, in solution; taking longer than three hours the total decomposition of the organics to carbon dioxide and water.

4. Conclusions

We report a new one-pot strategy for the preparation of enhanced dye-sensitized titanias, based in the *in-situ* co-condensation of tetrabutyl orthotitanate (TBOT) and adequately
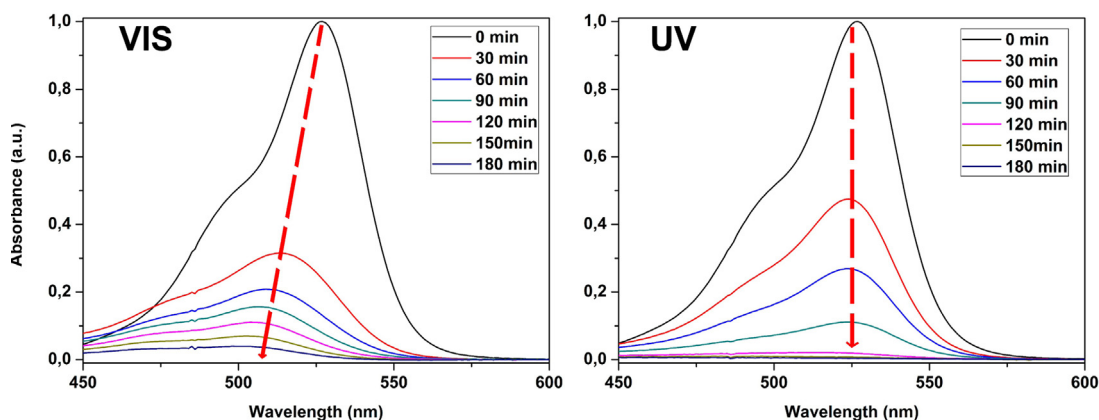
Fig. 12. UV–vis absorption spectra of the degradation reaction of an aqueous solution of R6 G ($5*10^{-5}$ M) under visible (left) or UV (right) irradiation using as photocatalyst TiO$_2$_Ir_IS.

functionalized coordination dyes. This synthesis approach allows the use of different photoactive metal complexes as building blocks, the neutral Ru(II) N3 dye and the cationic [Ir(ppy)$_2$(3,3′-H$_2$dcbpy)]PF$_6$, to produce new hybrid titanias based materials (**TiO$_2$_M_IS**) with anatase phase and a more efficient incorporation of the chromophores to the semiconductor matrix than that obtained by traditional post-synthetic grafting methods. This fact provides additional protection of the dyes, leading to an exceptional stability against both photodegradation and leaching, but still making them electronically accessible, and allowing their reusing as catalyst in fluid media for a long period of time. Also, the hybrid *in-situ* **TiO$_2$_M_IS** present a narrowing of the band gap associated with the indirect transitions of the anatase phase up to 0.42 eV in relation to control dye-free TiO$_2$. This combined effect improves remarkably their photocatalytic performance under UV or visible irradiation, as compared to the control titania and related grafted materials. This synthetic approach represents a new simple and standardisable strategy for the rational design of highly stable photoactive titania-based materials with great applicability potential in solar energy conversion devices. We are currently studying the incorporation of these materials to the electrode architecture of low-temperature sintered dye-sensitized solar cells (lt-DSSCs).

Acknowledgements

Appendix A. Supplementary data

Supplementary data associated with this article can be found, in the online version, at http://dx.doi.org/10.1016/j.apcatb.2016.06.061.

References

[1] X. Chen, A. Selloni, Chem. Rev. 114 (2014) 9281–9282.
[2] P.V. Kamat, J. Phys. Chem. C 116 (2012) 11849–11851.
[3] W.Y. Teoh, J.A. Scott, R. Amal, J. Phys. Chem. Lett. 3 (2012) 629–639.
[4] X. Chen, S.S. Mao, Chem. Rev. 107 (2007) 2891–2959.
[5] S. Min, F. Wang, Y. Han, J. Mater. Sci. 42 (2007) 9966–9972.
[6] L. Jianwei, Z. Peng, L. Ang, S. Fengli, W. Tuo, L. Yuan, G. Jinlong, Chem. Commun. 49 (2013) 5817–5819.
[7] X. Chen, L. Liu, P.Y. Yu, S.S. Mao, Science 331 (2011) 746–750.
[8] M.K. Nazeeruddin, M. Grätzel, Struct. Bond. 123 (2007) 113–175.
[9] A. Mishra, M.K.R. Fischer, P. Bauerle, Angew. Chem. Int. Ed. 48 (2009) 2474–2499.
[10] S.J. Wu, C.Y. Chen, J.G. Chen, J.Y. Li, Y.L. Tung, K.C. Ho, Dyes Pigm. 84 (2010) 95–101.
[11] S.-C. Yeh, P.-H. Lee, H.-Y. Liao, Y.-Y. Chen, C.-T. Chen, R.-J. Jeng, J.-J. Shuye, ACS Sustain. Chem. Eng. 3 (2015) 71–81.
[12] W. Yongzhen, Z. Wei-Hong, M.Z. Shaik, G. Michael, ACS Appl. Mater. Interfaces 7 (2015) 9307–9318.
[13] C. Sahin, D. Th, C. Varlikli, S. Icli, M.L.-S. Ch, Sol. Energy Mater. Sol. Cells 94 (2010) 686–690.
[14] N. Hirata, J.J. Lagref, E.J. Palomares, Chem. Eur. J. 10 (2004) 595–602.
[15] J. Singh, A. Gusain, V. Saxena, A.K. Chauhan, P. Veerender, S.P. Koiry, P. Jha, A. Jain, D.K. Aswal, A.K. Gupta, J. Phys. Chem. C 117 (2013) 21096–21104.
[16] J.H. Heo, S.H. Im, J.H. Noh, T.N. Mandal, C.S. Lim, J.A. Cahng, Y.H. Lee, H.J. Kim, A. Sarkar, M.K. Nazeeruddin, M. Grätzel, S.I. Seok, Nat. Photonics 7 (2013) 486–491.
[17] A. Yamamoto, K. Teramura, S. Hosokawa, T. Shishido, T. Tanaka, ChemCatChem 7 (2015) 1818–1825.
[18] C.-H. Lee, J.-L. Shie, C.-Y. Tsai, Y.-T. Yang, C.-Y. Chang, J. Clean Energ. Tech. 1 (2013) 115–119.
[19] G. Zhang, G. Kim, W. Choi, Energy Environ. Sci. 7 (2014) 954–966.
[20] M.K. Nazeeruddin, S.M. Zakeeruddin, R. Humpry-Baker, P. Jirousek, P. Liska, N. Vlachopoulos, V. Shklover, C.H. Fischer, M. Grätzel, Inorg. Chem. 38 (1999) 6298–6305.
[21] M. Rico-Santacruz, A.E. Sepúlveda, E. Serrano, E. Lalinde, J.R. Berenguer, J. García-Martínez, J. Mater. Chem. C 2 (2014) 9497–9504.
[22] E. Serrano, N. Linares, J. García-Martínez, J.R. Berenguer, ChemCatChem 5 (2013) 844–860.
[23] J.B. Waern, C. Desmarets, L. Chamoreau, H. Amouri, A. Barbieri, C. Sabatini, B. Ventura, F. Barigelletti, Inorg. Chem. 47 (2008) 3340–3348.
[24] M. Rico-Santacruz, A.E. Sepúlveda, E. Serrano, J.R. Berenguer, E. Lalinde J. García-Martínez, Spain Patent Number ES2539624 (2015), No. sol. 201300536, 2013.
[25] W. Jiang, Y. Gao, Y. Sun, F. Ding, Y. Xu, Z. Bian, F. Li, J. Bian, C. Huang, Inorg. Chem. 49 (2010) 3252–3260.
[26] L. Qin, H. Yang, C. Qin, Z. Xiang, M. Zhang, L. Ding, T. Yi, S. Yang, Dalton Trans. 42 (2013) 4790–4794.
[27] M.W. Perkovic, Inorg. Chem. 39 (2000) 4962–4968.
[28] I. Bratsos, S. Jedner, A. Bergamo, G. Sava, T. Gianferrara, E. Zangrando, E. Alessio, J. Inorg. Biochem. 102 (2008) 1120–1133.
[29] M. Nishio, Encyclopedia of Supramolecular Chemistry, in: J.L. Atwood, J.L. Steed (Eds.), Marcel Dekker Inc., New York, USA, 2004.
[30] R. Jose, A. Kumar, V. Thavasi, S. Ramakrishna, Nanotechnology 19 (2008) 424004, 7pp.
[31] U. Schubert, J. Mater. Chem. 15 (2005) 3701–3715.
[32] M.S. Lowry, W.R. Hudson, R.A. Pascal, S. Bernhard, J. Am. Chem. Soc. 126 (2004) 14129–14135.
[33] W.K. Seok, A.K. Gupta, S.J. Roh, W. Lee, S.H. Han, Bull. Korean Chem. Soc. 8 (2007) 1311–1316.
[34] P. Paoprasert, J.E. Laaser, W. Xiong, R.A. Franking, R.J. Hammers, M.T. Zanni, J.R. Schmidt, P. Gopalan, J. Phys. Chem. C 114 (2010) 9898–9907.
[35] M.K. Nazeeruddin, R. Humphry-Baker, P. Liska, M. Grätzel, J. Phys. Chem. B 107 (2003) 8981–8987.
[36] J. Zhu, D. Yang, J. Geng, D. Chen, Z.H. Jiang, J. Nanopart. Res. 10 (2008) 729–736.
[37] D. Zhao, C. Chen, W. Yang, H. Ji, W. Ma, L. Zang, J. Zhao, J. Phys. Chem. C 112 (2008) 5993–6001.
[38] A.E. Bocquet, T. Mizokawa, K. Morikawa, A. Fujimori, S.R. Barman, K. Maiti, D.D. Sarma, Y. Tokura, M. Onoda, Phys. Rev. B (1996) 1161–1170.
[39] G.W. Simmons, B.C. Beard, J. Phys. Chem. 91 (1987) 1143–1148.
[40] M. Oku, H. Matsuta, K. Wagatsuma, Y. Waseda, S. Kohiki, J. Elec. Spect. Rel. Phen. 105 (1999) 211–218.
[41] P. Stefanov, M. Shipochka, P. Stefchev, Z. Raicheva, V. Lazarova, L. Spassov, J. Phys. Conf. Ser. 100 (2008) 012039–012042.
[42] A.O.T. Patrocinio, E.B. Paniago, R.M. Paniago, N.Y.M. Iha, Appl. Surf. Sci. 254 (2008) 1874–1879.

[43] E. McCafferty, J.P. Wightman, Surf. Interface Anal. 26 (1998) 549–564.
[44] M. Balaraju, V. Rekha, B.L.A.P. Devi, R.B.N. Prasad, P.S.S. Prasad, N. Lingaiah, Appl. Catal. A: Gen. 384 (2010) 107–114.
[45] P. Reyes, M.C. Aguirre, I. Melián-Cabrera, M.L. Granados, J.L.G. Fierro, J. Catal. 208 (2002) 229–237.
[46] H. Rojas, G. Borda, P. Reyes, J.J. Martínez, J. Valencia, J.L.G. Fierro, Catal. Today 13–135 (2008) 699–705.

[47] Y. Wang, Z.H. Jiang, F. Yang, Mater. Sci. Eng. B 128 (2006) 229–233.
[48] T. Aarthi, G. Madras, Ind. Eng. Chem. Res. 46 (2007) 7–14.
[49] J. Yu, Q. Li, S. Liu, M. Jaroniec, Chem. Eur. J. 19 (2013) 2433–2441.
[50] T. Wu, G. Liu, J. Zhao, H. Hidaka, N. Serpone, J. Phys. Chem. B 102 (1998) 5845–5851.
[51] F. Chen, J. Zhao, H. Hidaka, Int. J. Photoen. 5 (2003) 209–217.
[52] P. Wilhelm, D. Stephan, J. Photochem. Photobiol. A: Chem. 185 (2007) 19–25.